the hamster cheek pouch. Circ Res **41:** 365-373, 1977
11. Whalen WJ, Nair P: Intracellular $PO_2$ and its regulation in resting skeletal muscle of the guinea pig. Circ Res **21:** 251-261, 1976.
12. Whalen WJ, Nair P: Skeletal muscle $PO_2$; effect of inhaled and topically applied $O_2$ and $CO_2$. Am J Physiol **218:** 973-980, 1970
13. Coburn RF, Mayers LB: Myoglobin $O_2$ tension determined from measurements of carboxymyoglobin in skeletal muscle. Am J Physiol **220:** 66-74, 1971
14. Duling BR: Microvascular responses to alterations in oxygen tension. Circ Res **31:** 481-489, 1972
15. Whalen WJ, Nair P, Buerk D, Thuning CA: Tissue $PO_2$ in normal and denervated cat skeletal muscle. Am J Physiol **227:** 1221-1225, 1974
16. McNeill TA: Venous oxygen saturation and blood flow during reactive hyperemia in the human forearm. J Physiol (Lond) **134:** 195-201, 1956
17. Eikens E, Wilcken DEL: Reactive hyperemia in the dog heart; effects of temporarily restricting arterial inflow and of coronary occlusions lasting one and two cardiac cycles. Circ Res **35:** 702-712, 1974
18. Olsson RA: Myocardial reactive hyperemia. Circ Res **37:** 263-270, 1975
19. Duling BR: Oxygen sensitivity of vascular smooth muscle. II. In vivo studies. Am J Physiol **227:** 42-49, 1974
20. Detar R, Bohr DF: Oxygen and vascular smooth muscle contraction. Am J Physiol **214:** 241-244, 1968
21. Carrier OC Jr, Walker JR, Guyton AC: Role of oxygen in autoregulation of blood flow in isolated vessels. Am J Physiol **206:** 951-954, 1964
22. Howard RO, Richardson DW, Smith MH, Patterson JL Jr: Oxygen consumption of arterioles and venules as studied in the Cartesian diver. Circ Res **16:** 187-196, 1965
23. Pittman RN, Duling BR: Oxygen sensitivity of vascular smooth muscle. I. In vitro studies. Microvasc Res **6:** 202-211, 1973
24. Dornhorst AC, Whalen RF: The blood flow in muscle following exercise and circulatory arrest; the influence of reduction in effective local blood pressure, of arterial hypoxia, and of adrenaline. Clin Sci **12:** 33-40, 1953
25. Olsson RA: Kinetics of myocardial reactive hyperemia blood flow in the unanesthetized dog. Circ Res **14/15** (suppl I): 81-86, 1964
26. Patterson GC: The role of intravascular pressure in the causation of reactive hyperaemia in the human forearm. Clin Sci **15:** 17-25, 1955
27. Hilton SM: Experiments on the post-contraction hyperaemia of skeletal muscle. J Physiol (Lond) **120:** 230-245, 1953
28. Kontos HA, Patterson JL Jr: Carbon dioxide as a major factor in the production of reactive hyperaemia in the human forearm. Clin Sci **27:** 143-154, 1965
29. Kontos HA, Mauck HP Jr, Patterson JL: Mechanism of reactive hyperemia in limbs of anesthetized dogs. Am J Physiol **209:** 1106-1114, 1965
30. Rubio R, Wiedmeier VT, Berne RM: Relationship between coronary flow and adenosine production and release. J Mol Cell Cardiol **6:** 561-566, 1974
31. Reivich M, Coburn R, Lahiri S, Chance B, (eds): Proceedings of the Symposium on Tissue Hypoxia and Ischemia, Philadelphia, August 1976. New York, Plenum, 1977

# Detection and Localization of Multiple Epicardial Electrical Generators by a Two-Dipole Ranging Technique

DAVID M. MIRVIS, FRANCIS W. KELLER, RAYMOND E. IDEKER, JOHN W. COX, JR., ROBERT F. DOWDIE, AND DAVID G. ZETTERGREN

**SUMMARY** **The ability of a numerical procedure to detect and to localize two experimentally induced, epicardial dipolar generators was tested in 24 isolated, perfused rabbit heart preparations suspended in an electrolyte-filled spherical tank. Electrocardiograms were recorded from 32 electrodes on the surface of the test chamber before and after placement of each of two epicardial burns. The second lesion was located either 180°, 90°, or 45° from the first. Signals were processed by iterative routines that computed the location of one or two independent dipoles that best reconstructed the observed surface potentials. The computed single dipole accounting for 99.68% of root mean square (RMS) surface potential recorded after the first burn was located 0.26 ± 0.10 cm from the centroid of the lesion. Potentials recorded after the second lesion were fit with two dipoles that accounted for 99.36 ± 1.51% of RMS surface potentials and that were located 0.42 ± 0.26 cm and 0.57 ± 0.49 cm from the centers of the corresponding burn. Seventy-one percent of computed dipoles were located within the visible perimeter of the burn. Thus, two simultaneously active dipolar sources can be detected and accurately localized by rigorous study of the generated electrical field.**



CLINICAL electrocardiography strives to semiquantitatively define the physiological state of the heart from the electrical potentials it generates. The concept of an equivalent cardiac generator has been useful in this effort. An equivalent cardiac generator may be defined[1] as a distribution of electrical sources in a specified volume conductor which generates potential distributions identical to, or "equivalent" to, those generated by the natural electrical generator, i.e., the heart. Many generator models have been proposed and tested in the search for a truly equivalent cardiac generator. The earliest and simplest generator was the fixed, single dipole model. Waller[2] idealized the relationships between the electromotive force of the heart and surface leads by considering the heart to be a lumped point source and point sink of current located within the cardiac region of the torso. Einthoven et al.[3] brought the source and sink pair close together to form an electrical doublet, or dipole.

From the Section of Medical Physics, Department of Medicine, University of Tennessee Center for the Health Sciences, Memphis, Tennessee.

Supported by Grants HL-01362, HL-09495, and HL-20597 from the National Heart, Lung and Blood Institute, National Institutes of Health, U.S. Public Health Service. Dr. Mirvis was supported in part by National Service Award HL-05323 from the National Heart, Lung and Blood Institute, National Institutes of Health.

Dr. Ideker's current address is the Department of Pathology, Duke University, Durham, North Carolina.

Address for reprints: David M. Mirvis, M.D., 951 Court Ave., Room 339M, Memphis, Tennessee 38163.

Received November 30, 1976; accepted for publication March 25, 1977.

Later, the dipole was permitted to be both eccentric and mobile, existing at different sites during various periods of the cardiac cycle,[4, 5] corresponding to the moving wavefronts observed in animal experiments using intramyocardial electrodes.[6, 7] The single moving dipole model has served as the basis for the "dipole ranging" technique developed in this laboratory.[8–13] This procedure computes the location as well as the orientation and magnitude of an equivalent cardiac generator from external potential measurements.

It became apparent, however, that a single dipole could not fully account for observed cardiac electrical activity. Direct studies of ventricular excitation in dog and man indicated that depolarization is a more complex process than can be explained by a single dipole.[6–7] During some portions of ventricular activation, two or more independent, simultaneously active wavefronts can be detected; it would be impossible to reconstruct these multiple electromotive surfaces if only a single resultant dipole were known. Body surface mapping has also provided evidence of nondipolarity of the cardiac generator. Taccardi[14, 15] and Horan et al.,[16] for example, documented multiple simultaneous minima and/or maxima; such patterns probably require more than dipolar sources.

Another source of data suggesting significant nondipolarity is the study of isolated, perfused animal hearts suspended in artificially constructed volume conductors. Reports from this laboratory with regard to turtle[10] and rabbit[17] hearts are representative. When relative dipolarity was assessed by inverse computation of the parameters of a single moving dipole, an average of 30% of root mean square (RMS) surface potential during the middle third of the QRS was nondipolar. In contrast, the first and last thirds of QRS were highly dipolar, as were the S-T segment and T wave.

One approach to developing a more adequate generator model was to visualize the heart as a multiple rather than as a single dipole source.[18, 19] A form of this greater-than-one dipole generator is the two-moving-dipole model.[20, 21] This solution has the intuitive appeal that each independently locatable dipole may be interpreted as representing a separate wavefront of myocardial electrical activity. In the study to be reported here, two epicardial burns, each representing a dipolar electrical generator, were placed at various sites on an isolated perfused rabbit heart. The ability of a two-dipole solution to localize these lesions accurately was then evaluated. In addition, results of this technique were compared with those using surface isopotential mapping, a second method capable of detecting multiple epicardial wavefronts.[14–16]

## Methods

### EXPERIMENTAL PROTOCOL

Twenty-four adult New Zealand white rabbits were stunned by a heavy blow to the occiput after systemic heparinization. The hearts were rapidly excised through a left thoracotomy and the cut ends of the aortic roots were tied to an electrically insulated perfusion cannula. This cannula passed vertically through one hemisphere of a previously described[10–12] spherical chamber measuring 6.350 cm in diameter. Perfusion of the isolated heart was immediately instituted with warmed, oxygenated Krebs-Henseleit solution at a perfusion pressure of 70 cm $H_2O$. The lower hemisphere of the tank was bolted in place, and the chamber was filled with additional warmed perfusate.

Electrocardiographic signals were simultaneously recorded from 32 silver-silver chloride electrodes on the inner surface of the sphere, paired to form 32 bipolar leads comprising a closed Kirchoff's loop.[10, 12] Electrodes were placed at the 20 vertices and at the centroids of the 12 facets of an underlying regular icosahedral reference figure. Signals were amplified by low noise (4 $\mu$V, peak-to-peak) differential amplifiers which were calibrated under computer control (PDP-7). The gain and DC offset of each amplifier were individually set by computer programming so that the incoming signal filled the input range of the analog-to-digital converter. Analog-to-digital conversion was performed on-line at a sampling rate of 2,500 samples/channel per second, and digital data were immediately recorded on a magnetic disc. Approximately 18 seconds of data were acquired during each recording session.

An initial set of data was acquired prior to performing any intervention. After data collection, the lower portion of the chamber was replaced by an accessory section containing a plane vertical glass plate. The chamber was refilled and five QRS-triggered photographs of the suspended heart were taken. The perfusion cannula was rotated 72° after each photograph to provide pictorial documentation of the position of the heart within the chamber.

Next, the accessory chamber section was removed. The epicardium of the anterior left ventricular free wall was seared[12] briefly with a heated soldering iron. The lower electrode-studded hemisphere was replaced, the chamber refilled with electrolyte, a second set of potentials recorded, and a second set of photographs taken (Fig. 1A).

A second burn was then made on the epicardium in 24 preparations. In eight, this lesion was placed on the posterior left ventricle, approximately 180° in rotation from the initial burn. In a second set of eight hearts, the second lesion was placed 90° from the first; in four this was on the left ventricular free wall and in four it was on the right

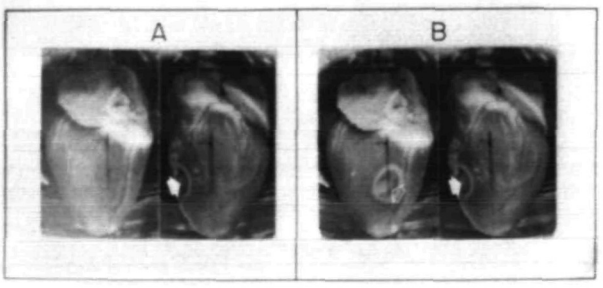


FIGURE 1 *Photographs of the suspended, perfused rabbit heart after placement of one (panel A) and of both (panel B) burns. The second view in each panel is after rotation of the heart 72° to the observer's left from the position in the first photograph. Cross-hairs mark the center of the experimental chamber. The two lesions are approximately 180° apart. Solid arrows identify the first lesion in the right photographs of each panel, and the open arrow identifies the second burn in the left photo of panel B.*

ventricular epicardium. In the third group of eight, the lesions were 45° apart; four were to the right and four were to the left of the initial burn. After the second burn was made, the recording and photographic procedures were repeated (Fig. 1B).

### DATA PROCESSING AND ANALYSIS

Off-line data processing was performed on two laboratory-oriented digital computer systems (PDP-7 and PDP-15).[10] Stability of the waveforms recorded during the 18-second data acquisition period was verified by an autocorrelation technique. Precision of the instrumentation system and, particularly, the accuracy of preamplifier calibration was checked by computing "closure error," a scalar directly proportional to the degree by which the sum of potentials recorded from leads forming a closed Kirchoff's loop deviated from the expected zero value. Closure errors of less than 0.5% were computed in a typical experiment.

Next, a series of QRST complexes, selected as being morphologically similar on the basis of autocorrelation values, were averaged to reduce random noise. Typically, 16 such complexes were averaged. These averaged waveforms for each bipolar lead were then reduced to unipolar form by referencing the potential of each electrode against the average potential of all 32 electrodes.

From these 32 unipolar potentials the parameters of a centric multipole series,[8] a single moving dipole model,[9] and the two independently locatable dipole models[20] were computed. The 24 parameters of a centric multipole series through the hexadecapole term were calculated as previously described.[8, 10] Three location and three moment terms of the single moving dipole that best reproduced the 32 electrode potentials were computed by an iterative procedure developed by Terry et al.[9] Thirty-two equations were constructed of the form

$$V_n = \frac{1}{4\pi\sigma}\left\{\left[\frac{2(Xn - X)}{r^3} + \frac{\frac{Xn - X}{r} + \frac{Xn}{R}}{Rr + R^2 - (XnX + YnY + ZnZ)}\right] Mx + \left[\begin{matrix}\text{Similar term} \\ \text{in Y}\end{matrix}\right] My + \left[\begin{matrix}\text{Similar term} \\ \text{in Z}\end{matrix}\right] Mz\right\} \quad (1)$$

where $V_n$ = recorded potential at electrode n; Xn, Yn, Zn = location coordinates of electrode n; X, Y, Z = location coordinates of computed dipole; Mx, My, Mz = X, Y, and Z moment components of computed dipole; r = distance between dipole and electrode; $\sigma$ = conductivity of conducting medium; and R = radius of sphere.

Inverse solution of this set of 32 equations yielded the location, orientation, and strength of the best single equivalent cardiac dipole.

Determination of the parameters of the two-dipole solution was likewise based on a series of 32 equations relating the potential recorded at each electrode site to the 12 parameters of the two-dipole model, i.e., X, Y, and Z location coordinates and Mx, My, and Mz moments for each dipole.[20, 21] The potential function for two moving dipoles, forming each of 32 equations, was recently derived by Martin et al.[20] and is a superposition of two equations of the form of Equation 1 as derived for a single eccentric dipole. Solution of this set of equations, linear with respect to moment but nonlinear with respect to location, relied upon the Marquardt algorithm,[22] an iterative scheme whereby each subsequent iteration produces a sum-squared residual potential smaller than the previous one. The routine was initialized with each of 500 randomly selected X, Y, and Z coordinates corresponding to points within the test chamber with eccentricities of less than 0.75. An identical set of initial guesses was used for all hearts and all time points studied. The operation proceeded until a minimum residual value was found or until a maximum of 40 iterations had been performed.

Isopotential maps of the potential distribution on the surface of the test chamber were constructed as previously described.[10, 23] The centric multipole series previously computed served as an interpolating function. Maps were drawn in views corresponding to the five photographs taken of each heart. Isopotential lines were typically drawn at 25-$\mu$V intervals.

A selected portion of the T-P segment was used as a baseline. Thus, injury currents generated by the epicardial burns appeared as S-T segment elevation.[12] For all computations, the entire chamber, including heart and perfusate, was assumed to be an electrically homogeneous volume conductor.

Heart photographs were used to determine the anatomic location of the burns. Five to nine points on the perimeter of each burn that were visible on at least two photographic views were selected, and the location of each point in three-dimensional space referenced to the center of the tank was calculated by triangulation. A circle was fit to these loci by a least squares technique. The center of this circle was considered to be the centroid of the injured area and the circumference to be its perimeter.

## Results

Points 10 msec after the termination of the QRS complex were selected for analysis. Prior to placing the first burn, maximum surface potential 10 msec into the S-T segment as determined from isopotential maps ranged from near zero to 50 $\mu$V.

### SINGLE BURNS

The initial burn, placed on the anterior left ventricular surface (Fig. 1A) measured 0.35 ± 0.03 cm in radius and was located at an eccentricity from the chamber's center of 0.45 ± 0.07. Unipolar recordings from electrodes overlying the lesion demonstrated significant S-T elevation whereas S-T depression was evident in those from electrodes on the opposite face of the chamber (Fig. 2A). Surface potential distributions were quantitatively highly dipolar, with 8.00 ± 3.78% of RMS potential not being attributable to a single dipole generator. Because RMS values were computed, the Pythagorean rather than the algebraic sum of fractions attributable and not attributable to a given generator must equal unity. Thus, 99.68% of RMS potential was attributable to a single dipole.

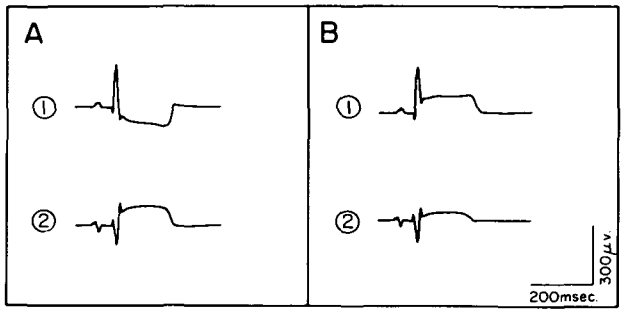


FIGURE 2 *Unipolar recordings from two electrodes after one (panel A) and after two (panel B) burns, in the same preparation as illustrated in Figure 1. Electrode 2 was aligned with the initial burn (panel A, Figure 1) and electrode 1 was aligned with the second lesion (panel B, Figure 1).*

The computed location of this best-fitting dipole was compared with the coordinates of the center of the burn, as determined photographically. Results are tabulated in Figure 3. The mean distance from the burn center to the locus of the equivalent dipole (line C-D in Figure 3) was 0.25 ± 0.10 cm. When the computed dipole was projected onto the plane of the burn margin, its displacement from the burn center (line C-D' in Figure 3) was 0.22 ± 0.09 cm. The angle between the computed dipole and a vector normal to the plane of the burn (angle $M_D$-$N_C$, Figure 3) was 9.4 ± 5.0 degrees.

## DUAL BURNS

The second burn was similar in size (0.35 ± 0.03 cm, radius) to the first and located at a similar eccentricity (0.42 ± 0.09). Waveforms derived from electrodes overlying the second lesion demonstrated S-T elevation, whereas some previously had illustrated reciprocal S-T depression (Fig. 2A and B).

From the 500 initial guesses used for each preparation, 395.5 ± 139.0 initializations converged upon computed dipole pairs located within the chamber, whereas 77.8 ± 128.0 initial guesses caused the iterative process to proceed to the maximum number of iterations permitted without successful convergence. The remaining 26.7 ± 24.5 converged upon points beyond the tank's boundaries. The latter two sets of data were eliminated from further evaluation.

In three experiments, a single pair of dipole loci was computed from the initial guesses successfully converging upon a point within the test chamber. Two independent pairs (Fig. 4) were determined in 14 preparations, three pairs in three, four pairs in two, five pairs in one, and seven pairs in one study. The pair accounting for the greatest percentage of RMS surface potential was the pair located nearest to the burn centers in 23 of the 24 preparations. In the remaining case, the sum of the distances from the dipoles to the corresponding burn centers was 0.24 cm greater with the dipole pair having the lowest potential residual than with the nearest pair.

A two-dipole model fit 99.36 ± 1.51% of RMS potential recorded after both burnings, with a residual of 7.27 ± 7.25%. Geometric relationships between the burn centers

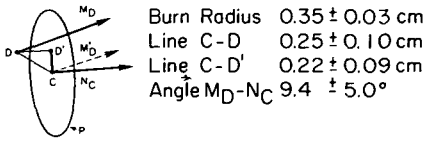


FIGURE 3 *Comparisons of photographically documented burn locations and computed dipole coordinates for the initial burn using a single dipole ranging technique. Magnitudes are means ± 1 standard deviation. C = centroid of visible perimeter (P) of burn; D = computed dipole location; D' = projection of point D on to plane of burn rim; $M_D$ = moment of computed dipole; $M'_D$ = moment $M_D$ translated to centroid of lesion; and $N_C$ = vector perpendicular to plane of burn.*

and the coordinates of the dipole pair with the lowest residual potential are presented in Table 1. Data presented were derived using the computed dipole pair with the lowest RMS potential residual. Distances from the centroid of the first burn to the nearest dipole and from the centroid of the second to the other dipole (line C-D) were 0.42 ± 0.26 and 0.57 ± 0.49 cm, respectively. After dipoles were projected to the plane of the corresponding burn, their displacements (line C-D') were 0.35 ± 0.25 and 0.40 ± 0.36 cm, respectively; 71% of the 48 dipoles were then located within the perimeter of the corresponding lesion. The remaining dipoles were located 0.39 ± 0.34 cm from the nearest boundary. Magnitudes of the angle $M_D$-$N_C$ for the two cases were 21.8 ± 14.7 and 35.2 ± 38.0 degrees.

The large standard deviations described were attributed in part to data derived from one preparation. Distances from burn centers to dipole locations in this heart were 1.3 and 2.3 cm. No procedural or other definable causes for the aberrancy were detectable. If these data were excluded, magnitudes of lines C-D, C-D', and angle $M_D$-$N_C$ for the first burn of the remaining 23 preparations were

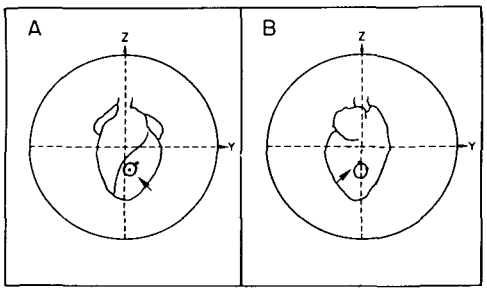


FIGURE 4 *Distribution of dipole loci computed for the preparation illustrated in Figures 1 and 2. The view in panel B corresponds to a 216° rotation of the heart as viewed in panel A. Positions of the computed dipoles are indicated by dots, and the burns by the circled areas on the superimposed cardiac silhouette. The first burn is seen in panel A and the second in panel B. Arrows identify the dipole loci nearest to the centers of the respective burns. Positive ends of Y and Z axes of a three-dimensional Cartesian coordinate system are indicated by the horizontal and vertical dashed lines, respectively. The two dipoles so identified are 0.23 and 0.39 cm from the burn centers and account for all but 5.1% of observed root mean square (RMS) surface potential. The remaining pair are 0.46 and 0.63 cm from the burn centers; 5.8% of RMS surface potential was not accounted for by this pair.*

TABLE 1 *Localization of Two Epicardial Burns by a Two-Dipole Ranging Technique*

| | First burn | Second burn |
|---|---|---|
| Burn radius | 0.35 ± 0.03 cm | 0.40 ± 0.03 cm |
| Burn eccentricity | 0.45 ± 0.07 | 0.42 ± 0.09 |
| Line C-D | 0.42 ± 0.26 cm | 0.57 ± 0.49 cm |
| Line C-D′ | 0.35 ± 0.25 cm | 0.40 ± 0.36 cm |
| Angle $M_D$-$N_C$ | 21.8 ± 14.7° | 35.2 ± 38.0° |

All values are means ± 1 SD.

Abbreviations are as in Figure 3: line C-D = distance from center of lesion to located dipole; line C-D′ = distance from projection of computed dipole onto the plane of burn rim to center of lesion; angle $M_D$-$N_C$ = angle, in degrees, between vector perpendicular to plane of burn and dipole moment vector.

0.38 ± 0.18 cm, 0.31 ± 0.19 cm, and 41.8 ± 10.9°, respectively. For the second burn, corresponding values were 0.50 ± 0.31 cm, 0.35 ± 0.29 cm, and 40.7 ± 34.5°.

The distance from the center of the first burn to the corresponding dipole computed after placing the second burn and using the two-dipole model was 0.11 ± 0.28 cm greater ($P > 0.1$) than that computed with but one lesion present using a single dipole method. No significant differences were found in the accuracy of the two-dipole technique in localizing the first and the second burn ($P > 0.1$). In addition, the second burn was as accurately located regardless of its direction and distance from the first lesion. The distances from the burn centers to the projections of the dipole to the plane of the burn (line C-D′, Figure 3) were 0.32 ± 0.22, 0.36 ± 0.03, and 0.38 ± 0.16 cm for the 180°, 90°, and 45° subgroups, respectively ($P >$ 0.1, all comparisons).

## ISOPOTENTIAL MAPPING

Isopotential maps drawn after the first epicardial lesion was produced demonstrated a single maximum spatially aligned with the photographically documented burn location (Fig. 5). A single minimum was noted on the opposite tank surface. Intensity of the maximum exceeded that of the minimum consistent with an eccentric dipole generator.

After the second lesion was placed, two maxima appeared when the two lesions were separated by 180° or 90°. Each maximum was spatially aligned with the corresponding epicardial burn (Fig. 5). In preparations with the second burn 45° from the first, a single maximum was observed in a location intermediate between sites predicted for the maxima due to the two lesions (Fig. 6). The maximum observed with one burn shifted toward that expected of the second burn and increased in magnitude.

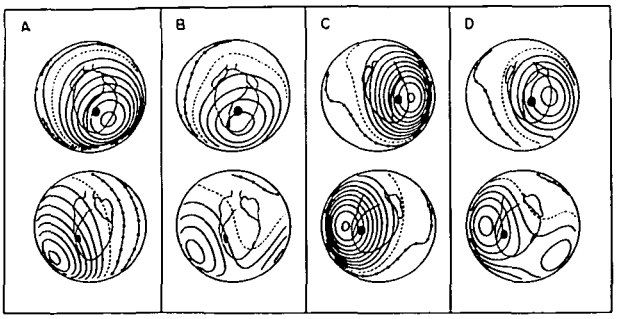


FIGURE 5 *Isopotential distribution on the surface of the experimental chamber, superimposed upon tracings of the cardiac silhouette. Contour lines are drawn at 25-μV intervals, with positive potentials indicated by solid lines, negative potentials by boxed lines, and the zero potential contour by the dashed line. Burns are identified by the solid black areas. Panels A and B: Distribution in two views separated by 72° with one burn (panel A) and with both burns (panel B) in the same preparation illustrated in Figures 1, 2, and 4. Lesions were separated by 180°. Panels C and D: Potential patterns after one burn (panel C) and after two burns (panel D) in a preparation in which the second lesion was located 90° from the first on the left ventricular free wall.*

## Discussion

Gabor and Nelson,[5] in 1954, demonstrated that the strength, location, and orientation of the resultant dipole of a system of sources and sinks in a volume conductor could be determined by integration of potentials recorded over the bounding surface. The first moment of the distribution gives the magnitude and orientation of the dipole while the second moment quantitates its location. A second approach to locating a single dipole was proposed by Geselowitz[24] in 1960, and was shown to be similar to that of Gabor and Nelson by Brody.[8] It was documented that translation of a single dipole from the origin of the volume conductor reference system generates multipolar terms, as defined by a series of "shift equations." Inverse solution of these equations permits determination of dipole location. More recently, a method based upon the iterative solution of equations defining the potential generated at any surface point by an eccentric dipole was developed.[9] This procedure yields exact (less than 1% error) replication of dipoles with eccentricities up to 0.75. In contrast, dipole locations computed from quadripolar shift equations were accurate for eccentricities of 0.3 or less.[9]

The physiological accuracy of these procedures has been documented in three studies from this laboratory using isolated heart preparations. First, severing the right bun-

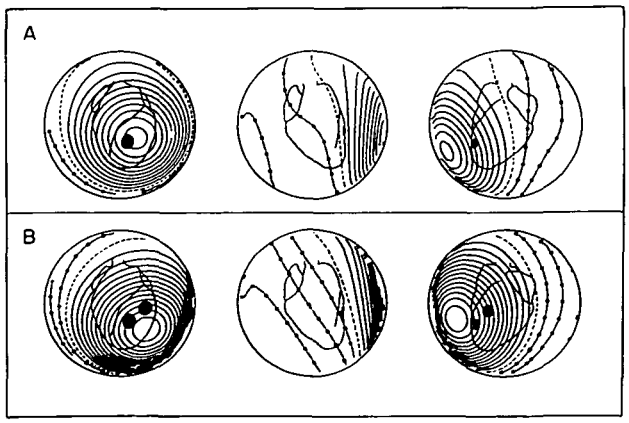


FIGURE 6 *Isopotential distribution in one preparation after placement of one burn (panel A) and after placing a second lesion 45° from the first on the left ventricular free wall (panel B). Cardiac silhouettes are superimposed, with burns demarcated. In each panel, the second and third views correspond to a rotation of the first view 72° and 288° to the observer's left. Contour lines are at 25-μV intervals; all markings are as in Figure 5.*

dle branch caused the position of the cardiac dipole to shift to the right side of the heart during the terminal QRS, consistent with delayed activation of the right free wall as expected with right bundle branch block.[11] Next, the precision of the technique in localizing experimentally induced dipolar generators was tested.[12] Both epicardial searing and subepicardial pacing were used as dipole generators. The computed dipole was located an average of 3.2 mm from the grossly visible center of the burn and 3.7 mm from the tip of the stimulating electrode. Last, this technique was used to compute heart vector location throughout spontaneous and ectopically paced cardiac cycles.[13] Results demonstrated the ability of computed heart dipole location to depict graphically the motion of an ectopic impulse across the heart. Qualitatively similar results have been presented by Gastonguay and Nelson[25] using the isolated frog gastrocnemius muscle, by Nelson et al.[26] using human torso models, and by Horan et al.,[27] Arthur et al.,[28] and Titomer[29] using human body surface recordings.

The methodology employed in the current study, designed to test a two-dipole ranging technique, was similar to that used in the prior studies validating the single dipole ranging method. An isolated heart system including a volume conductor of known geometry and precisely located electrodes greatly simplified computational procedures while reducing the effects of electrical inhomogeneity.[10, 12] The photographic system provided an alternate method of locating the lesions against which results of the numerical technique were compared. Expansion of the electrode array from 20, as in prior studies, to 32 permitted construction of sufficient simultaneous equations to compute hexadecapole parameters as well as the parameters of a two-dipole or a dipole-quadripole equivalent generator model. Simulation experiments reported by Martin et al.[20, 21] suggested that 32 simultaneous observations are the minimum needed for accurate solution of the two-dipole model.

Epicardial searing produces anatomically stationary injury current generators. Potentials generated are highly dipolar in form and remain stable over the experimental period. For example, surface maps constructed immediately and 30 minutes after a single burn are identical in form and differ in peak potential by only 25 $\mu$V.[23] However, difficulties do exist. First, the electrical center of the lesion is assumed to be in the anatomic center of the visible burn. This is indeed unlikely because of nonuniformity of contact pressure and heat around the rim of the lesion; definition of the exact electrical center would be possible only if epicardial electrograms were recorded, but is considered to be within the perimeter of the burn. Thus, computed dipole locations were compared not only with the centroid of the lesion but with the coordinates defining its bounds. Second, inhomogeneities, although minimized in this preparation, may cause an inward displacement of computed dipoles when compared to true locations.[12] This translocation accounted for almost one-half of the distance between the center of an epicardial burn and an inversely computed dipole locus in a previous study.[12] In an attempt to compensate for this effect, the distance from the burn center to the projection of the computed dipole to the plane of the burn rim was computed, as well as the absolute distance between the two loci.[12]

An additional source of error is the generation of octapolar components as dipolar forces are distributed over an electromotive surface.[8, 31] This causes dislocation of the two computed dipoles from their true loci in an attempt to account for these higher order terms. Thus, a more exact solution would be attainable with a true two-dipole source, rather than a two-dipolar electromotive surface model. The error introduced is small, however, if the surfaces have simple rim configurations, as with epicardial burns.[8]

Quantitation of the strength, location, and orientation of two independent dipoles requires solution of sets of simultaneous nonlinear equations. The nonlinear nature of these equations necessitates the use of complex optimization or minimization[20, 21, 30] routines which begin with a given "initial guess" as to the locations of the two dipoles. Electrode potentials that would be produced by such dipoles are compared to the observed electrode potentials, and the sum-squared (SSQ) residual is computed. An iterative scheme then adjusts the estimated dipole locations until the SSQ residual is minimized.

One difficulty with such minimization routines is that it is difficult to differentiate between local and global SSQ residual minima.[20, 30] In the former case, multiple sets of "best" dipole locations may be identified, depending upon the initial guess used. To circumvent this problem, the routines were initialized with 500 randomly determined dipole loci. It was hoped that only a few pairs of dipole locations would be found and that the pair with the lowest SSQ residual would represent the global minimum. Results verified this. The pair of dipoles producing the lowest SSQ residual was the one with the lowest mean distance from the two burn centers to the corresponding dipole loci in 23 of 24 cases.

The routines employed did, however, perform admirably despite these theoretical and practical difficulties. The initial burn was precisely localized using the single dipole ranging routine, as previously reported,[13] and the two-dipole method functioned as well in locating two lesions as did the single dipole technique in describing a single source. Additionally, lesions were as accurately detected and localized, regardless of separation and position on the heart surface. Thus, these mathematical routines may serve as one method to evaluate multiple, independent epicardial wavefronts.

Isopotential surface mapping is a second procedure capable of detecting multiple cardiac wavefronts.[14–16, 23] Current interpretative methods, however, permit only qualitative estimation of the location, strength, and character of the operative sources, and may, indeed, fail to detect multiple events with certain combinations of source strengths, eccentricities, and separations.[23, 32, 33] As illustrated in Figure 6, two burns separated by 45° generate a single maximum. Although the pattern mapped after two searings differs from that observed after the first, there is no suggestion that this alteration is due to the activation of a second source rather than the modification of the first. In contrast, the two lesions were localized by the ranging method to within the visible perimeter of the burn. It may be argued that the two lesions placed near to each other

act as a single large lesion. This cannot be excluded without direct epicardial recordings. However, two simulated, mathematically exact dipoles located in a bounded spherical volume conductor generate a field with a single maximum when separated by 45° at eccentricities of 0.25–0.67.[23] Thus, fusion of dipolar electromotive surfaces is not required to produce the type of surface pattern observed here.

These data therefore suggest that, under certain specified experimental or physiological circumstances, rigorous mathematical processing of surface potentials may provide a more accurate description of epicardial events than does visual inspection of isopotential patterns. Computational and theoretical difficulties caused by complex surface boundaries and tissue inhomogeneities may, however, limit application of these methods to intact animal protocols. Studies such as these using a controlled and simplified, but fundamentally physiological preparation do serve to test procedures at a level intermediate between purely mathematically defined simulation studies on one hand and less regulated in situ heart studies on the other. If a method were unsuccessful under these simplified conditions, it would be unlikely to function well in more complex physiological environments.

## References


1. Geselowitz DB: Dipole theory in electrocardiography. Am J Cardiol **14:** 301-306, 1964
2. Waller AD: On the electromotive changes connected with the beat of the mammalian heart and of the human heart in particular. Philos Trans R Soc Lond [Biol Sci] **180:** 169-194, 1889
3. Einthoven W, Fahr G, and DeWaart A: Über die Richtung und die manifeste Grösse der potentialschwankungen im meschlichen Herzer und über des Einfluss der Herzlage auf die Form de Elektrokardiogramms. Pfluegers Arch **150:** 275-315, 1913
4. Wilson FN, and Bayley RH: The electrical field of an eccentric dipole in a homogeneous spherical volume conductor. Circ Res **1:** 84-92, 1953
5. Gabor D, and Nelson CV: Determination of the resultant dipole of the heart from measurements on the body surface. J Appl Phys **25:** 413-416, 1954
6. Scher AM, Young AC, Malmgren AC, and Patton RP: Spread of electrical activity through the wall of the ventricle. Circ Res **1:** 539-547, 1953
7. Spach MS, and Barr RC: Ventricular intramural and epicardial potential distributions during ventricular activation and repolarization in the intact dog. Circ Res **37:** 243-275, 1975
8. Brody DA: The inverse determination of simple generator configurations from equivalent dipole and multipole information. IEEE Trans Biomed Eng **15:** 106-110, 1968
9. Terry FH, Brody DA, Eddlemon CO, Cox JW Jr, Keller FW, and Phillips HA: Dipole, quadripole and octapole measurements in isolated beating heart preparations. IEEE Trans Biomed Eng **18:** 139-147, 1971
10. Brody DA, Warr OS III, Wennemark JR, Cox JW Jr, Keller FW, and Terry FH: Studies of the equivalent cardiac generator behavior of isolated turtle hearts. Circ Res **29:** 512-524, 1971
11. Brody DA, Cox JW Jr, Keller FW, and Wennemark JR: Dipole ranging in isolated rabbit hearts before and after right bundle branch block. Cardiovasc Res **8:** 37-45, 1974
12. Ideker RE, Bandura JP, Larsen RA, Cox JW Jr, Keller FW, and Brody DA: Localization of heart vectors produced by epicardial burns and ectopic stimuli. Circ Res **36:** 105-112, 1975
13. Ideker RE, Bandura JP, Cox JW Jr, Keller FW, Mirvis DM, and Brody DA: Path and significance of heart vector migration during QRS and ST-T complexes of ectopic beats in isolated perfused rabbit hearts. Circ Res **41:** 558-564, 1977
14. Taccardi B: Distribution of heart potentials on dog's thoracic surface. Circ Res **11:** 862-869, 1962
15. Taccardi B: Distribution of heart potentials on the thoracic surface of normal human subjects. Circ Res **12:** 341-352, 1963
16. Horan LG, Flowers NC, and Brody DA: Body surface potential distribution; comparison of naturally and artificially produced signals as analyzed by digital computer. Circ Res **13:** 373-387, 1963
17. Cox JW Jr, Brody DA, Keller FW, Bandura JP, Dowdie RF, and Larsen RA: Direct experimental comparison of three inverse electrocardiographic constructs. Circulation **52** (suppl II): 67, 1975
18. Lynn MS, Barnard ACL, Holt JH, and Sheffield LT: A proposed method for the inverse problem in electrocardiology. Biophys J **7:** 925-945, 1967
19. Rogers CL, and Pilkington TC: Free-moment current dipoles in inverse electrocardiography. IEEE Trans Biomed Eng **15:** 312-323, 1968
20. Martin RO, Cox JW Jr, Keller FW, Terry FH, and Brody DA: Equivalent cardiac generators; two moving dipoles and moving dipole and quadripole. Ann Biomed Eng **2:** 164-183, 1974
21. Martin RO, Keller FW, Cox JW Jr, and Brody DA: A comparative study of nonlinear equivalent cardiac generators. Ann Biomed Eng **3:** 47-61, 1975
22. Marquardt DW: An algorithm for least-squares estimations of nonlinear parameters. J Soc Indust Appl Math **11:** 431-441, 1963
23. Mirvis DM, Ideker RE, Keller FW, Cox JW Jr, Zettergren DG, and Dowdie RF: Values and limitations of surface isopotential mapping techniques in the detection and localization of multiple discrete epicardial events. J Electrocardiol (in press)
24. Geselowitz DG: Two theorems concerning the quadrupole applicable to electrocardiography. IEEE Trans Biomed Eng **12:** 164-168, 1965
25. Gastonguay PR, and Nelson CV: Method for measuring dipole parameters of isolated hearts and muscles; application to frog gastrocnemius. IEEE Trans Biomed Eng **15:** 289-297, 1968
26. Nelson CV, Hodgkin BC, and Voukydis PC: Determination of the locus of the heart vector from body surface measurements. J Electrocardiol **8:** 135-146, 1975.
27. Horan LG, Flowers NC, and Miller CB: A rapid assay of dipolar and extradipolar content in the human electrocardiogram. J Electrocardiol **5:** 211-224, 1974
28. Arthur RM, Geselowitz DB, Briller SA, and Trost RF: The path of the electrical center of the human heart determined from surface electrocardiograms. J Electrocardiol **4:** 29-33, 1971
29. Titomer LI: Measurement of certain equivalent quadripole components of the equivalent electrical generator of the heart. Biophys J **14:** 403-411, 1969
30. Spang HA III: A review of minimization techniques for nonlinear functions. J Soc Indust Appl Math **4:** 343-365, 1962
31. Brody DA, and Bradshaw JC: The equivalent generator components of uniform double layer. Bull Math Biophys **24:** 183-195, 1962
32. De Ambroggi L, Taccardi B: Current and potential fields generated by two dipoles. Circ Res **27:** 901-911, 1970
33. Abildskov JA, Burgess MJ, Lux RL, Wyatt RF: Experimental evidence for regional cardiac influence in body surface isopotential maps of dogs. Circ Res **38:** 386-391, 1976